Supporting Information

Exploring the Multifunctionality of Co and Ni Selenospinels: Unveiling Co_3Se_4 as an Efficient Trifunctional Electrocatalyst for Glycerol, Hydrazine, and Water Oxidation Reactions

Diya Raveendran[a], Viplove Mishra[a], Avishek Roy[a], Supriti Pakhira[a], Arnab Sadhukhan[a], Aditi Chandrasekar[b], and Venkataramanan Mahalingam[a]**

[a]Department of Chemical Sciences, Indian Institute of Science Education and Research Kolkata, Mohanpur, West Bengal-741246, India

[b]School of Arts and Sciences, Azim Premji University, Bangalore-562125, India

*E-mail: mvenkataramanan@yahoo.com

*E-mail: aditi.chandrasekar@apu.edu.in

Experimental Section

Physical Characterizations

Powder X-ray diffraction (PXRD):

The Powder X-ray diffraction was conducted using a Rigaku MiniFlex 600 instrument equipped with a D/tex ultra detector to determine the phase of the as-prepared materials. The instrument utilized an X-ray source with Cu(Kα) (λ = 0.154 nm), a 2.5-degree solar slit, and a K-beta filter. All measurements were performed at an operating tube voltage of 40 kV and a tube current of 15 mA. Initially, all samples (including as-synthesized and post-catalytic materials) were placed on a quartz holder, and their diffraction patterns were recorded using Miniflex Guidance software (Version 3.1.6.0). The scan speed was set to 2°/min within the 2θ range of 10 - 80°. The raw data were analyzed using X-Pert HighScore software (Panalytical).

Field emission scanning electron microscopy (FESEM):

Sample Preparation:

A small amount of the as-prepared materials was dispersed in methanol via ultrasonication. A portion of this solution was drop-cast onto freshly cleaned silicon wafers and dried in a vacuum desiccator overnight. For post-electrochemical analyses, materials on carbon paper (CP) substrates were dried thoroughly and used directly.

Sample Coating:

Before FESEM imaging, samples were gold (Au) coated using a Quorum 150R ES Rotary Pumped Coater. The sputter current was maintained at 10 mA with a sputter time of 50 seconds, and a tooling factor of 2.30.

High-resolution transmission electron microscopy (HRTEM):

Sample preparation:

A small quantity of powder was dispersed in methanol and ultrasonicated for 15 minutes. The dispersion was then drop-cast onto a carbon-coated Cu grid (TED PELLA, 300 mesh) and dried in a vacuum desiccator. The dried Cu grids were analyzed directly with the HRTEM. All HRTEM analyses was done using Gatan Digital Micrograph software (Ametek).

Contact Angle measurement:

Sample preparation:

All the prepared materials were transformed into thin pellets using a hydraulic pellet maker set-up. Subsequently, the pellets were subjected to hydrophilicity studies.

Details of Electrochemical Studies

Preparation of the Working Electrode:

For GOR, 4 mg of catalyst was dispersed in 380 µL ethanol, then 20 µL Nafion binder solution was added. The mixture was sonicated, and 160 µL was drop-casted on each side of a 1 × 1 cm^2 carbon paper (CP), which was then dried. The catalyst loading was approximately 3.2 mg/cm^2.

For HzOR and OER, 2 mg of catalyst was dispersed in 190 µL ethanol, with 10 µL Nafion added. After sonication, 40 µL was drop-casted on each side of a 0.5 × 0.5 cm^2 CP, then dried. The catalyst loading was also about 3.2 mg/cm^2.

Electrochemical Parameters:

Ohmic drop (*i*R drop) compensation:

Before converting to the RHE scale, all measured potentials were manually 100% iR corrected to account for the ohmic drop (uncompensated resistance, Ru), following equation 1:

$$\mathbf{E\ (V) = E_{RHE}\ (V) - [(Current\ density(mA) / 1000) \times R_u\ (V)]} \text{ ----------(1)}$$

Cyclic Voltammetry (CV):

CV curves were recorded within their respective voltage ranges under non-stirring conditions. Electrochemical activation involved 20 CV cycles at 100 mV/s. The catalytic performance was then evaluated at 5 mV/s within the same potential window. All CV curves were manually 100% iR corrected and converted to the RHE scale using equations 2 and 3:

$$\mathbf{E(RHE) = E_{ref} + 0.059\ pH + E\ (Hg/HgO)} \text{ ----------(2)}$$

$$\mathbf{E(RHE) = 0.098 + 0.059\ pH + E\ (Hg/HgO)} \text{ ----------(3)}$$

Potentials required to reach specific current densities were estimated from the forward LSV curve for GOR and HzOR, and the backward LSV curve for OER.

Chronopotentiometry (CP):

CP measurements were conducted in the respective electrolytes, with stirring for GOR and without stirring for HzOR and OER, at designated current densities. Potentials were manually 100% iR corrected afterwards.

Tafel Slope Estimation:

Tafel slopes were derived from the LSV curves using the Tafel equation:

$$\mathbf{\eta = a + b\ log(j)} \text{ ----------(4)}$$

where η is the overpotential, a is an adjustable parameter, b is the Tafel slope (mV/dec), and j is the current density (mA/cm^2_{geo}). The Tafel slope was determined by selecting appropriate current density regions on the manually iR-corrected LSV curves.

Double-layer Capacitance (C_{dl}):

CV curves were recorded in non-faradaic regions (-0.03 to 0.03 V vs. OCP) at scan rates from 5 to 100 mV/s. The current density at OCP (V_{OCP}) was plotted against scan rates, and the slope of this plot provided the C_{dl} values.

Electrochemical Active Surface Area (ECSA):

ECSA was calculated using equation 5:

$$\mathbf{ECSA = C_{dl} / C_s} \text{ ----------(5)}$$

where C_s is the specific capacitance. For a 1 cm^2 flat electrode surface, the C_s value varies between 0.02 to 0.06 mF/cm^2 of ECSA. Here, we consider 0.04 mF/cm^2 of ECSA as the C_s value.

Electrochemical Impedance Spectroscopy (EIS):

EIS measurements were performed at a fixed potential specific to each reaction to obtain Nyquist plots. The semicircle observed within 200 kHz to 10 MHz corresponds to the charge transfer resistance (R_{ct}), deduced from the semicircle's diameter.

Error Estimation:

LSV experiments were repeated at least three times, and the standard deviation was used to calculate the potential error via equation 6.

$$S = \sqrt{\frac{\sum_{i=1}^{n} (x_i - z)^2}{n-1}} \text{ ----------(6)}$$

S = standard deviation of a sample, n = the number of measurements, X_i = the measured values of the sample at an i^{th} time, and Z = the mean value of all the measurements.

Construction of Alkaline Electrolyzer

For OHzWS and OWS:

Electrolysis tests were performed in a single-compartment glass cell with two electrodes: Co_3Se_4/CP as the anode and 20% Pt/C as the cathode. The cell was purged with Ar gas to eliminate dissolved oxygen before measurement, with continuous Ar flow maintained during testing to ensure accuracy. CV was recorded within the applicable voltage window, and catalytic activity was measured at different current densities.

For OGWS:

Water splitting with biomass upgrading was conducted in an H-type cell with continuous Ar supply to the cathodic chamber to prevent dissolved oxygen interference. A Nafion (212) membrane was used to separate the cathodic (consisting of 20% Pt/C/CP) and anodic (consisting of Co_3Se_4/CP) chambers. For the comparison in electrolyzer performance, the alkaline water splitting was also conducted in the H-type cell configuration under identical reaction conditions.

Reduced Energy Consumption:

Reduced energy consumption was calculated using equation 7:

$$Reduced\ energy\ consumption\ = \frac{(Cell\ voltage\ of\ OER - Cell\ voltage\ of\ alternative\ reaction) \times Current}{Cell\ voltage\ of\ OER \times Current}$$

----------(7)

^{1}H NMR quantification of organic product:

Sample preparation:

After bulk electrolysis, the entire electrolyte (10 mL) was collected, mixed with 0.1 M DMSO (internal standard required = 71 µL for 10 mL electrolyte), and sonicated well. Subsequently, 50 µL of the resultant aliquot solution was mixed with 550 µL of D_2O solvent and subjected to NMR spectroscopy.

Supporting Figures

Characterization

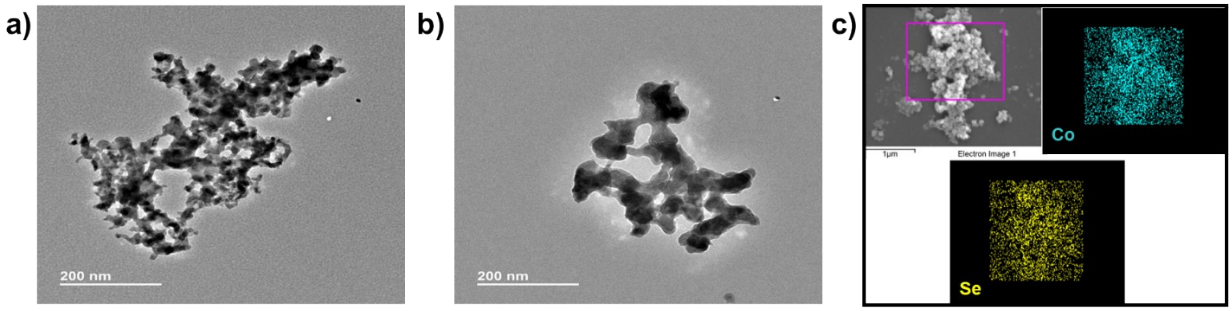

Figure S1. Structural and morphological characterizations. TEM images of (a) Co_3Se_4, (b) Ni_3Se_4. Elemental mapping of (c) Co_3Se_4.

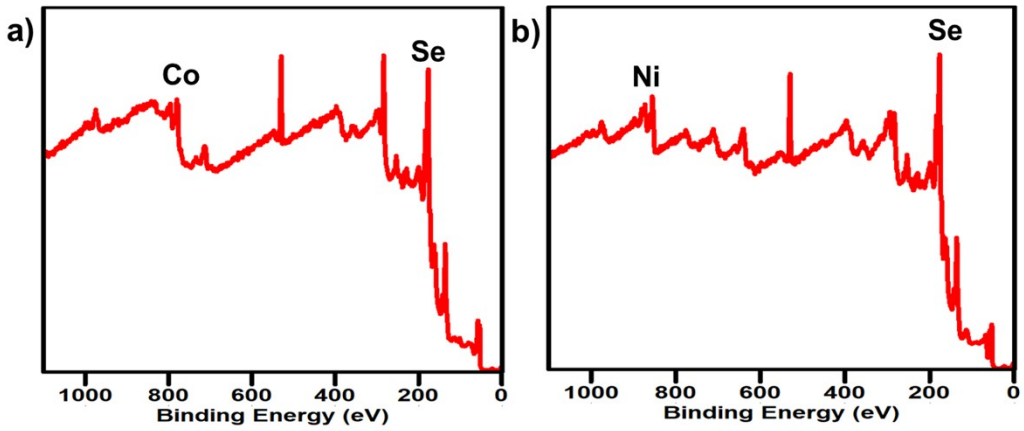

Figure S2. XPS survey spectra of a) Co_3Se_4, b) Ni_3Se_4.

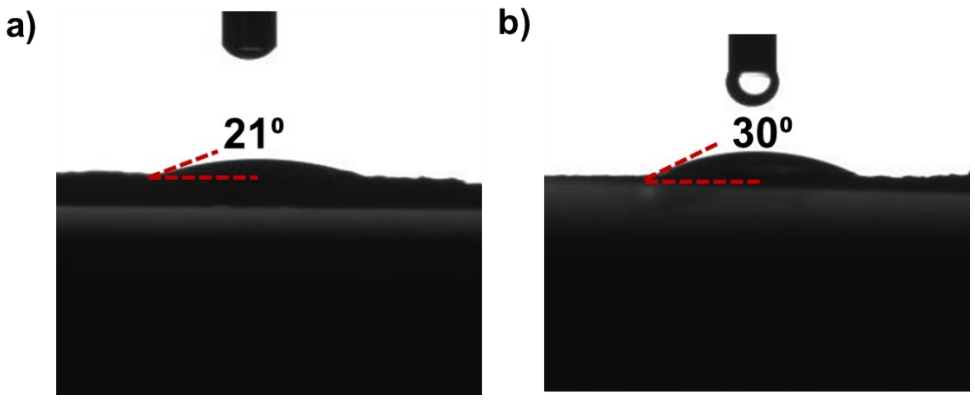

Figure S3. The contact angle test results of a) Co_3Se_4, b) Ni_3Se_4.

Experimental data for GOR

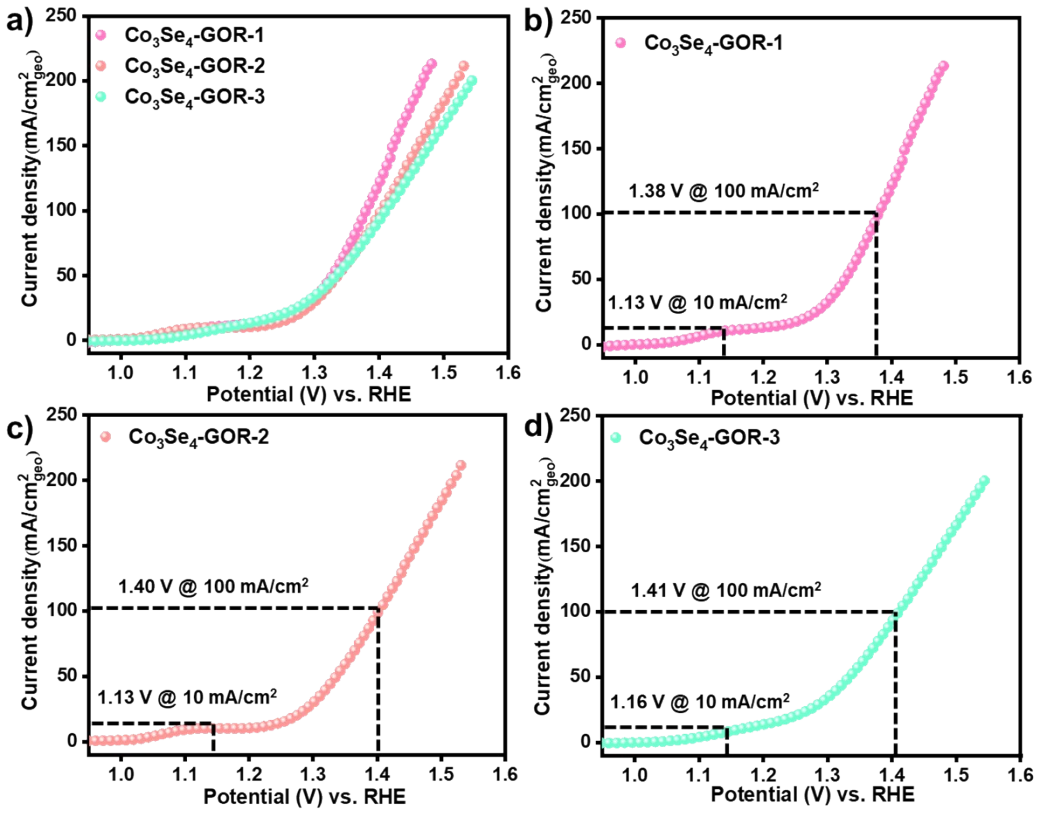

Figure S4. Reproducibility of electrocatalytic performance of Co_3Se_4 toward GOR in 0.1 M Glycerol + 1 M KOH with a standard deviation of 17 mV and 15 mV at 10 and 100 mA/cm^2, respectively.

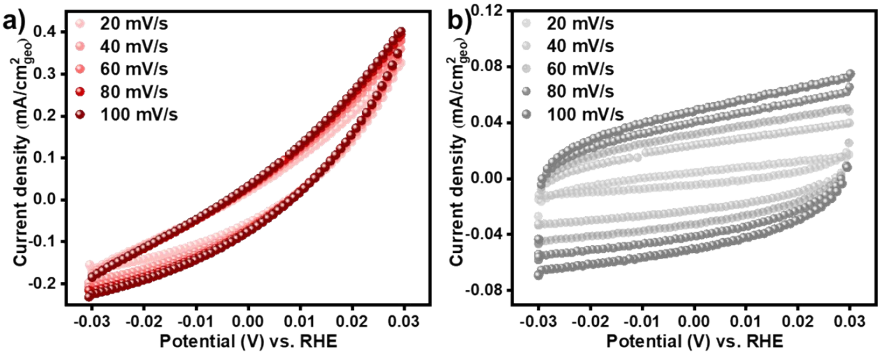

Figure S5. CVs of (a) Co_3Se_4 and (b) Ni_3Se_4 for GOR at different scan rates and in the non-faradaic potential region.

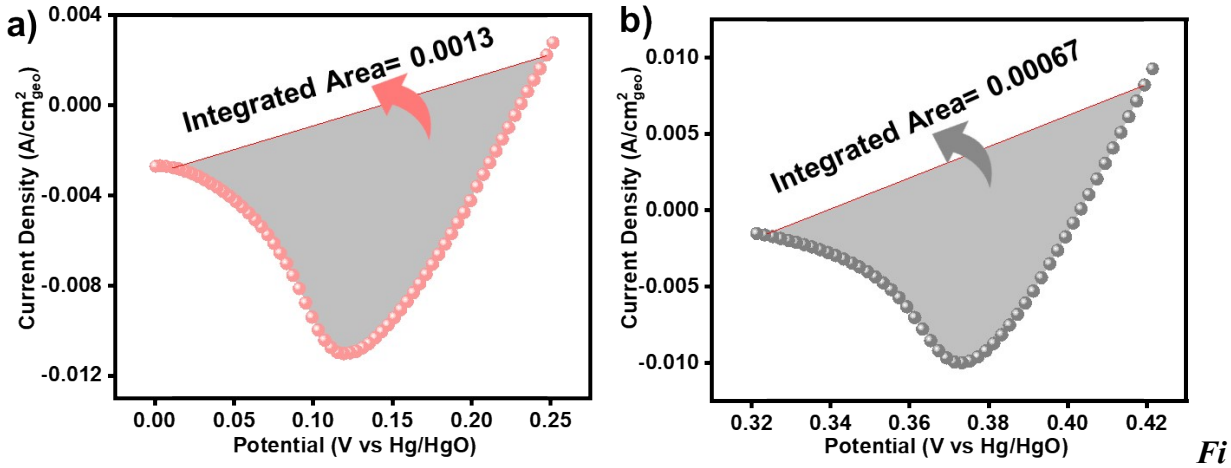

Figure S6. The area under the reduction peak from the CV graph of (a) Co_3Se_4 and (b) Ni_3Se_4.

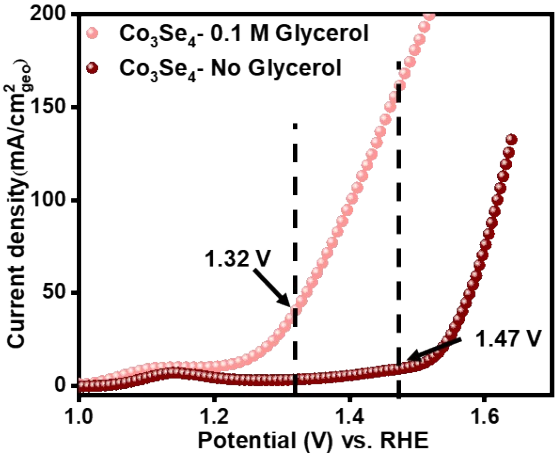

Figure S7. LSV curves displaying potential range (1.32 – 1.47 V vs RHE) where water oxidation is minimal and the organic oxidation reaction (OOR) is predominant in the case of Co_3Se_4/CP.

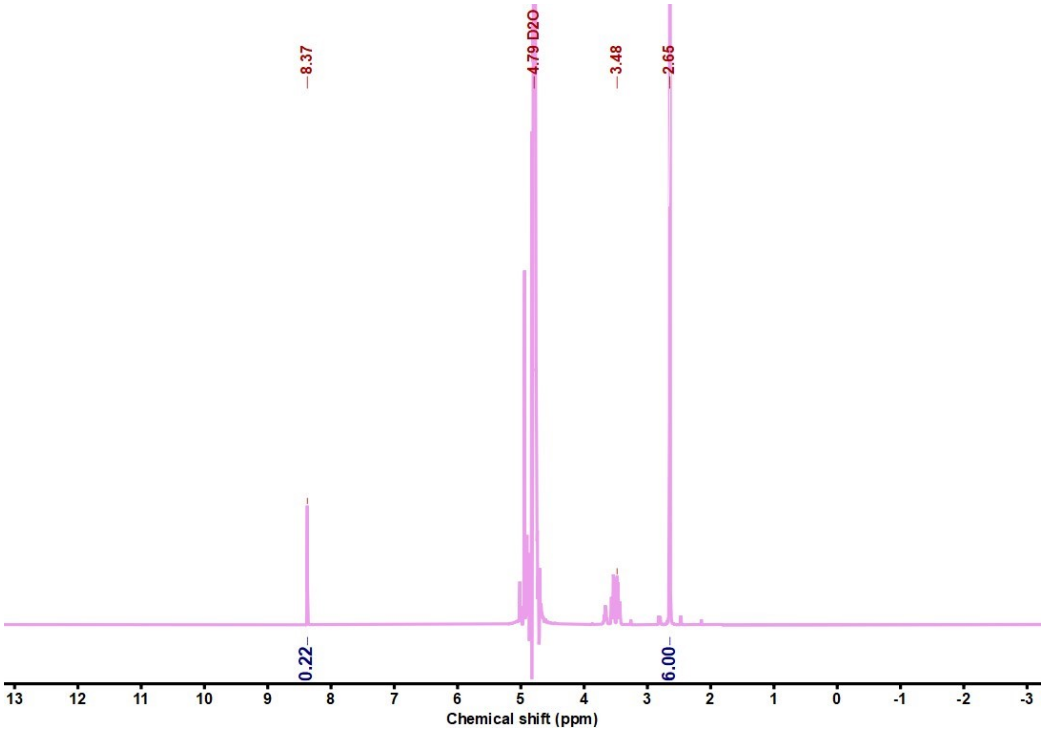

Figure S8. ^{1}H NMR spectrum of reaction mixture after glycerol oxidation using Co_3Se_4/CP as the anode material via 2 h CA at 1.32 V_{RHE}.

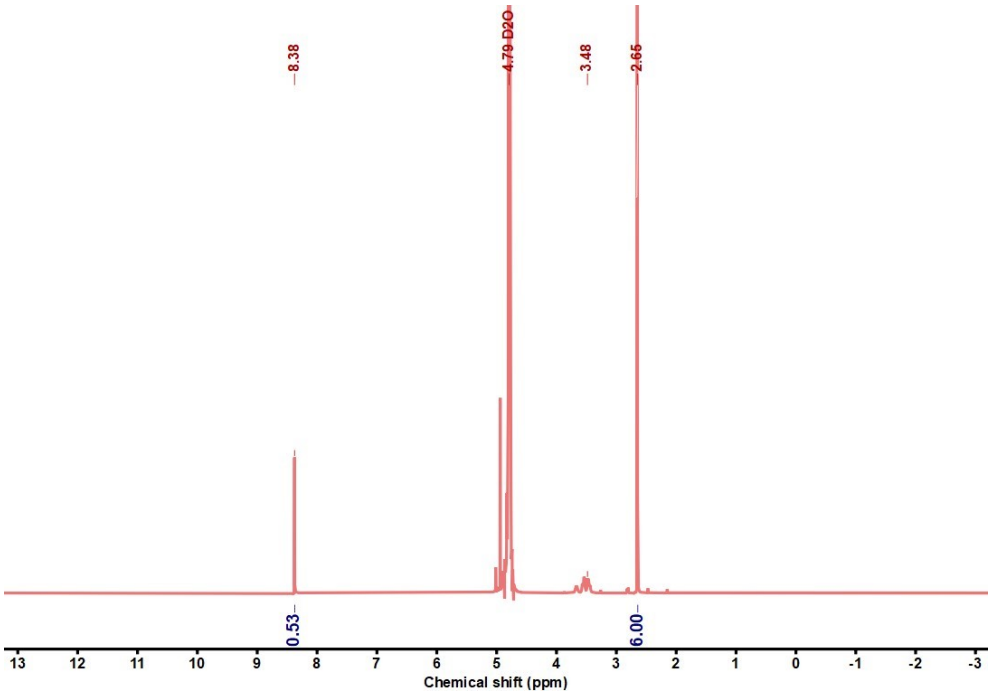

Figure S9. ^{1}H NMR spectrum of reaction mixture after glycerol oxidation using Co_3Se_4/CP as the anode material via 2 h CA at 1.37 V_{RHE}.

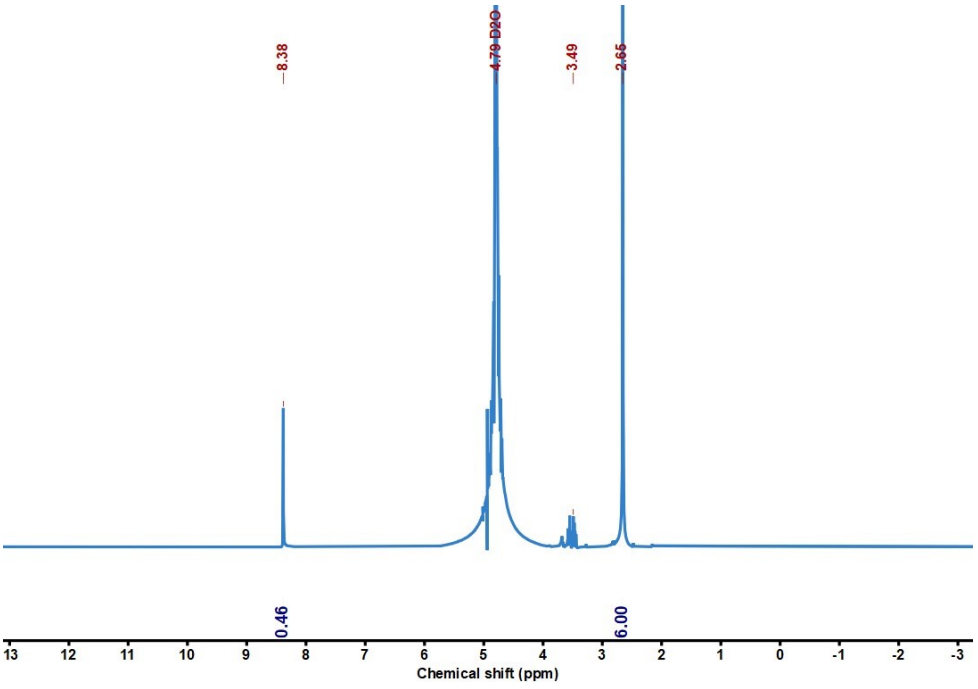

Figure S10. ^{1}H NMR spectrum of reaction mixture after glycerol oxidation using Co_3Se_4/CP as the anode material via 2 h CA at 1.42 V_{RHE}.

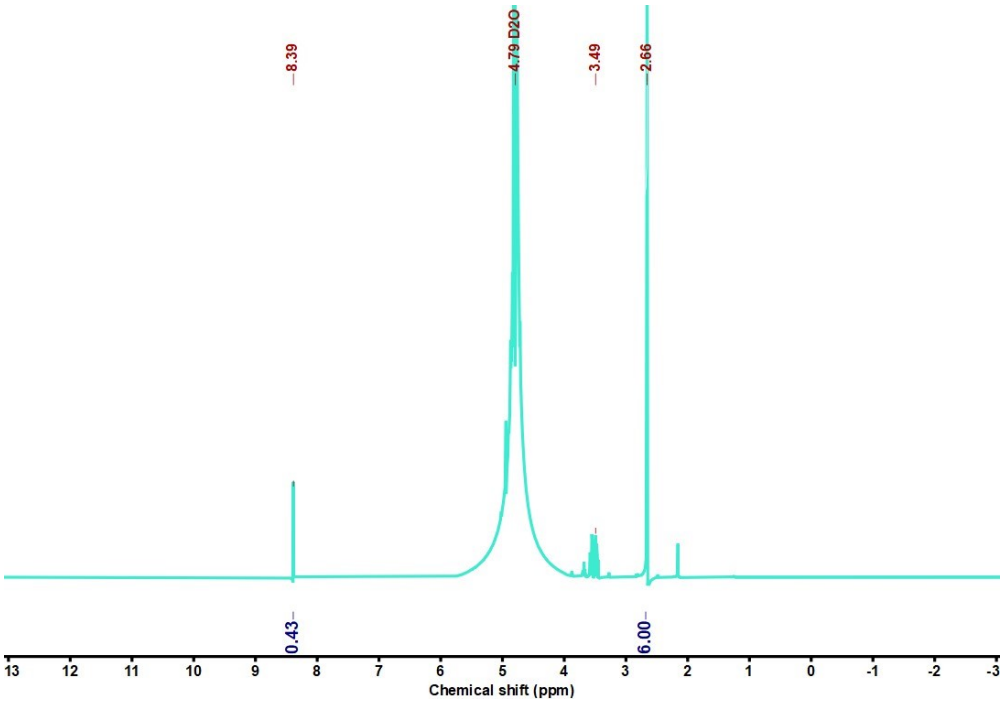

Figure S11. ^{1}H NMR spectrum of reaction mixture after glycerol oxidation using Co_3Se_4/CP as the anode material via 2 h CA at 1.47 V_{RHE}.

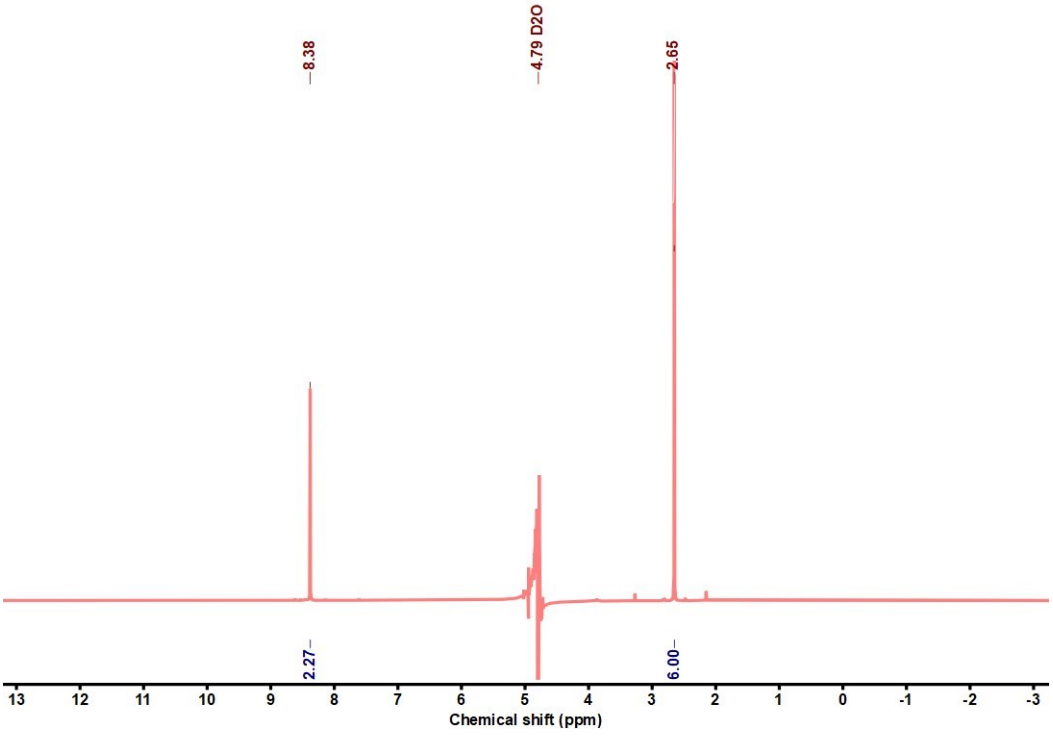

Figure S12. ^{1}H NMR spectrum of reaction mixture after bulk glycerol oxidation using Co_3Se_4/CP as the anode material via 12 h CA at 1.37 V_{RHE}.

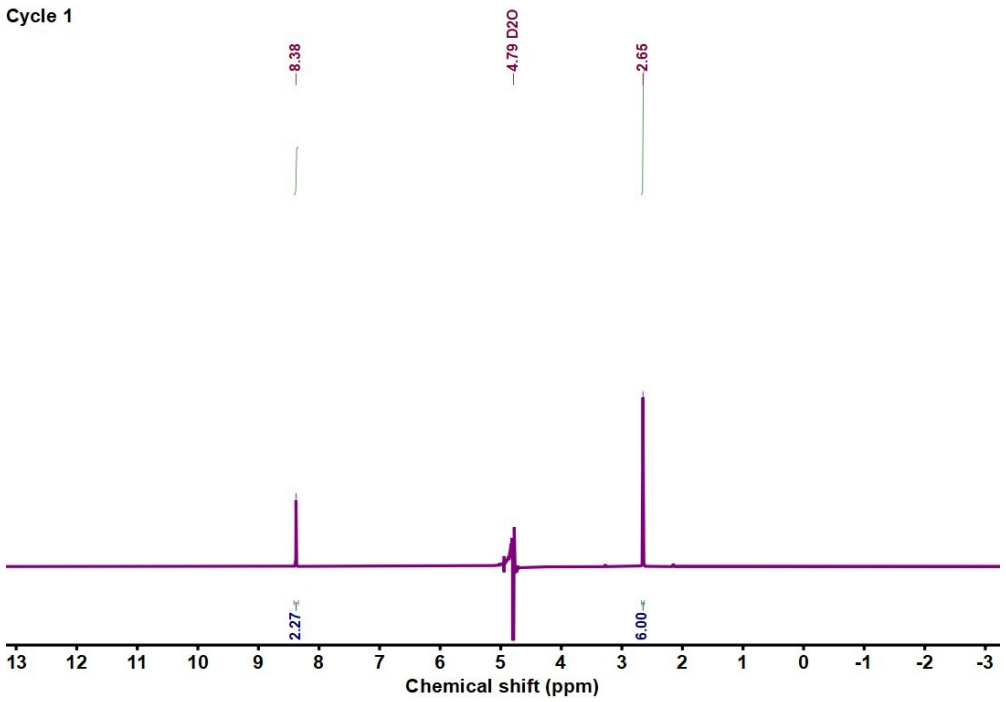

Figure S13. ^{1}H NMR spectrum of the reaction mixture after the first CA (12 h at 1.37 V_{RHE}) cycle of the reproducibility test, bulk glycerol oxidation using Co_3Se_4/CP as the anode.

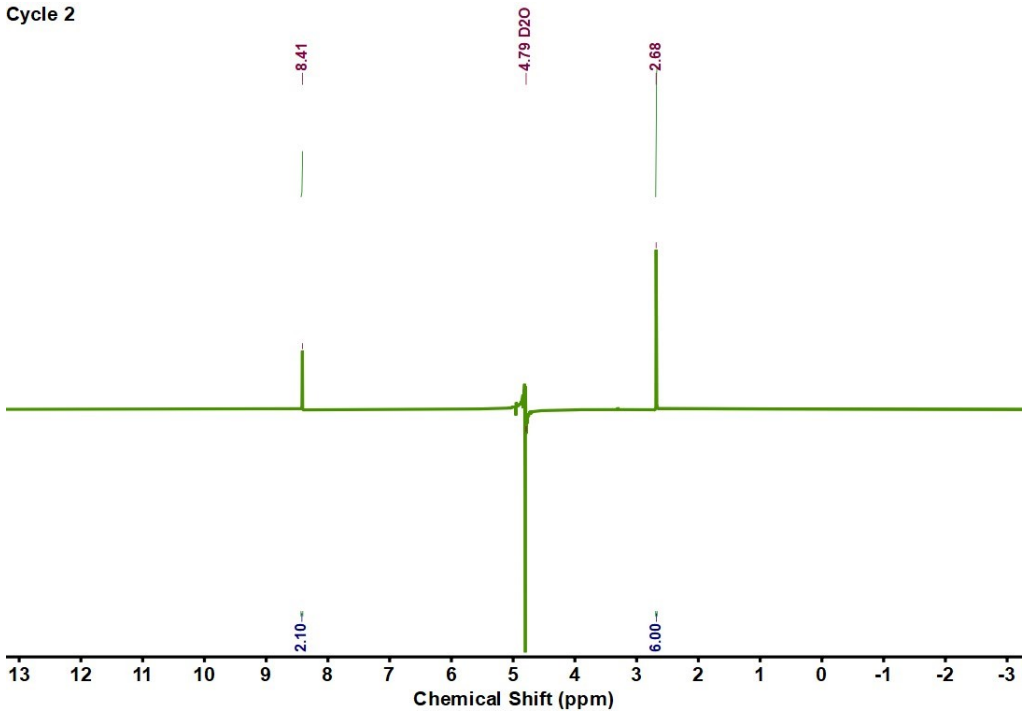

Figure S14. ^{1}H NMR spectrum of the reaction mixture after the second CA (12 h at 1.37 V_{RHE}) cycle of the reproducibility test, bulk glycerol oxidation using Co_3Se_4/CP as the anode.

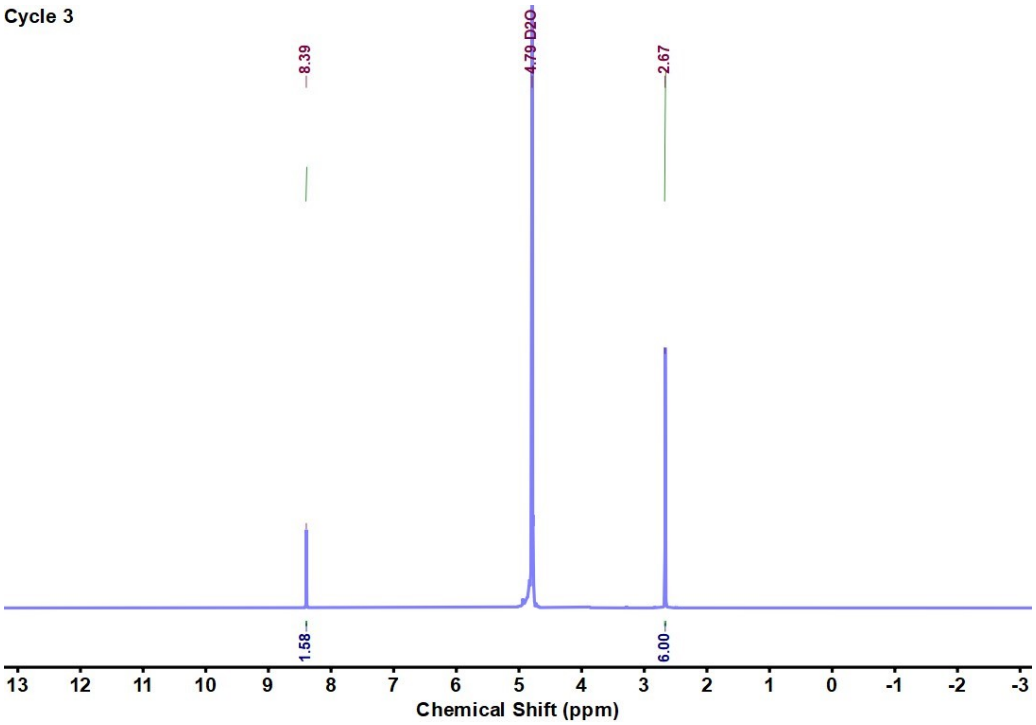

Figure S15. ^{1}H NMR spectrum of the reaction mixture after the third CA (12 h at 1.37 V_{RHE}) cycle of the reproducibility test, bulk glycerol oxidation using Co_3Se_4/CP as the anode.

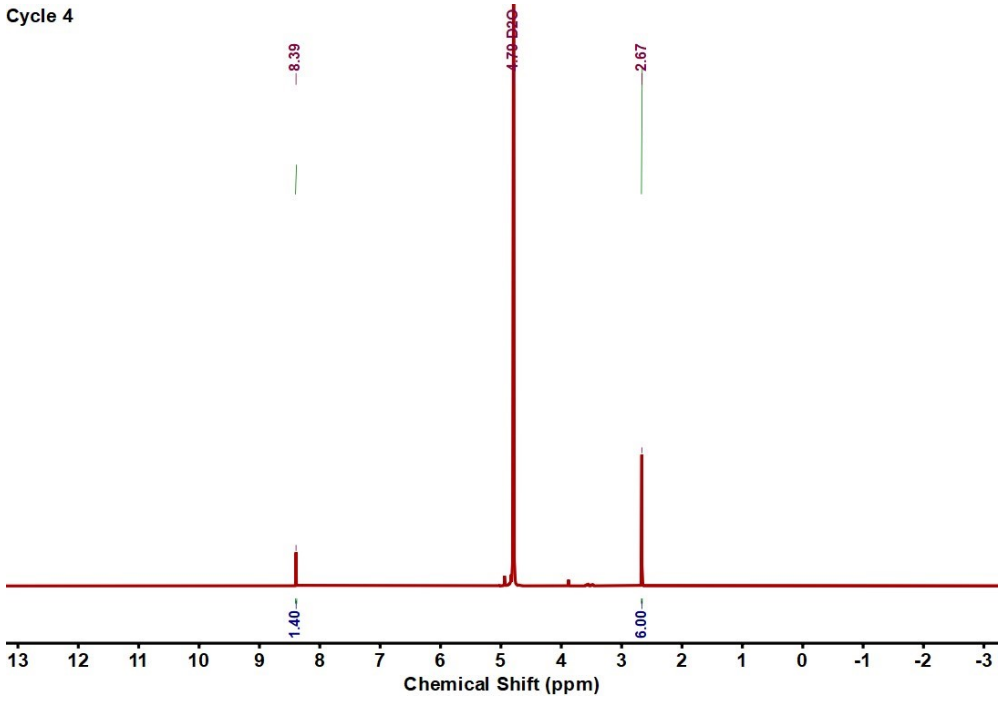

Figure S16. ^{1}H NMR spectrum of the reaction mixture after the fourth CA (12 h at 1.37 V_{RHE}) cycle of the reproducibility test, bulk glycerol oxidation using Co_3Se_4/CP as the anode.

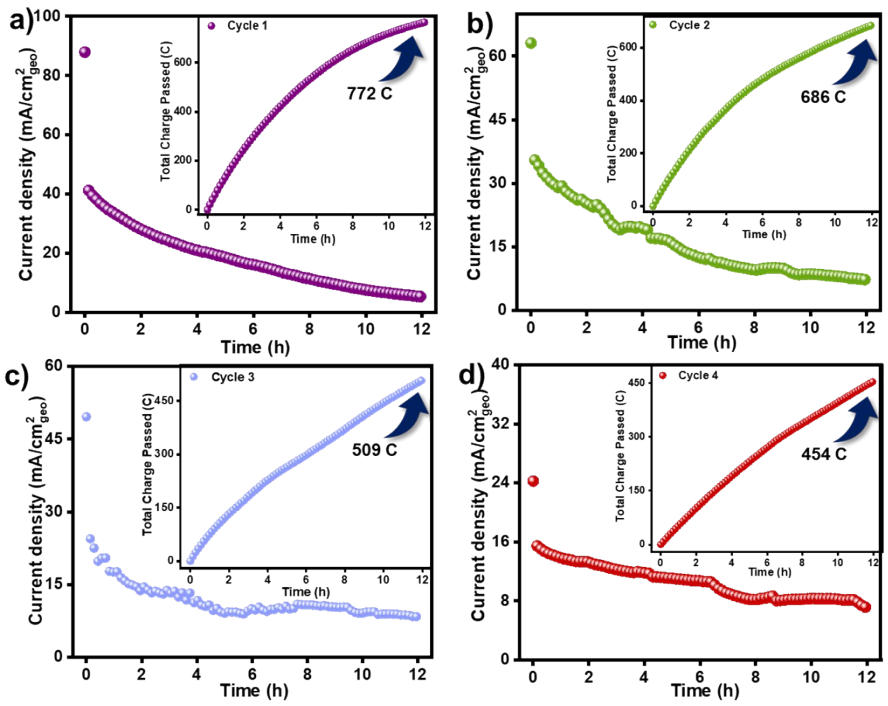

Figure S17. CA curves for the consecutive bulk electrolysis for 4 cycles in 0.1 M glycerol +1 M KOH for 12 h (inset: total charge passed during CA).

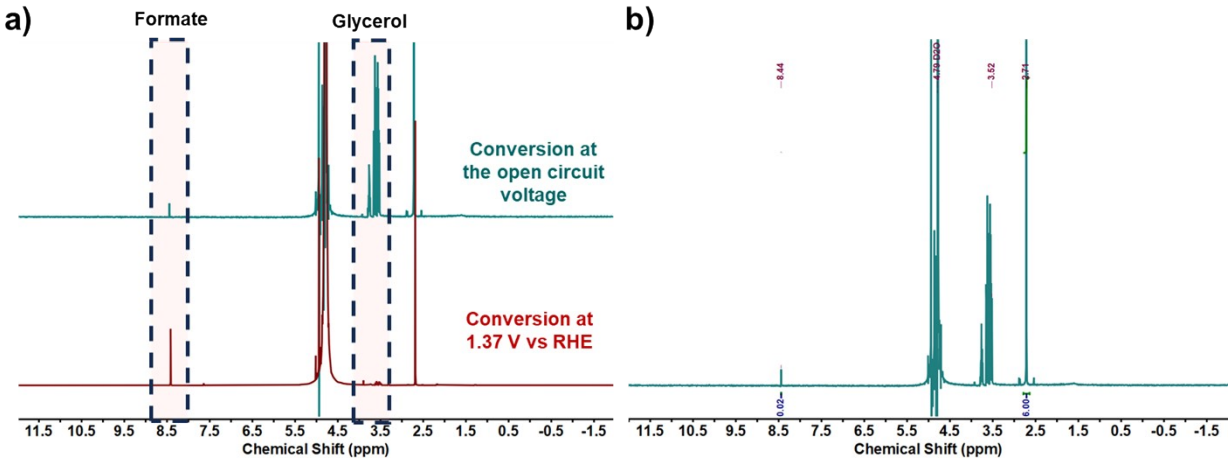

Figure S18. a) Comparison of the ^{1}H NMR spectrum of the reaction mixture after 12 h OCV and 12 h CA (12 h at 1.37 V_{RHE}). b) ^{1}H NMR spectrum of the reaction mixture after 12 h OCV with peak analysis.

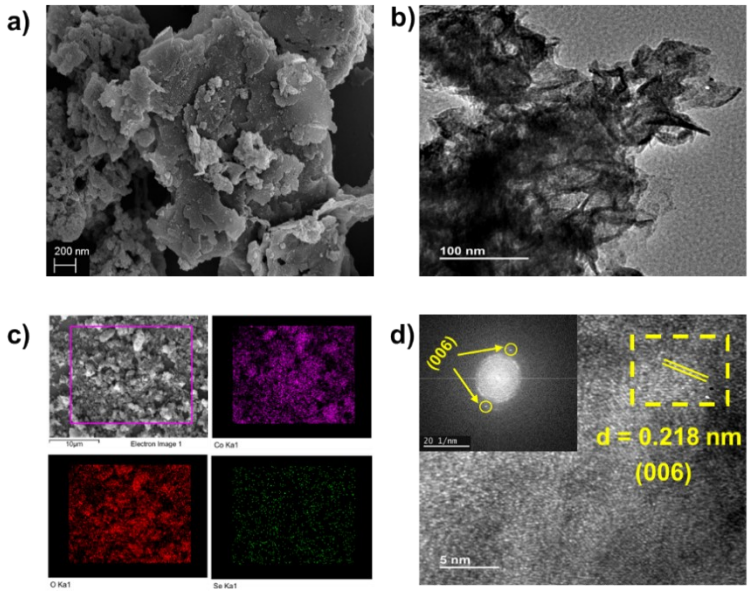

Figure S19. Post GOR catalysis characterization via (a) SEM, (b) TEM, (c) Elemental mapping, (d) HR-TEM (inset: Corresponding FFT).

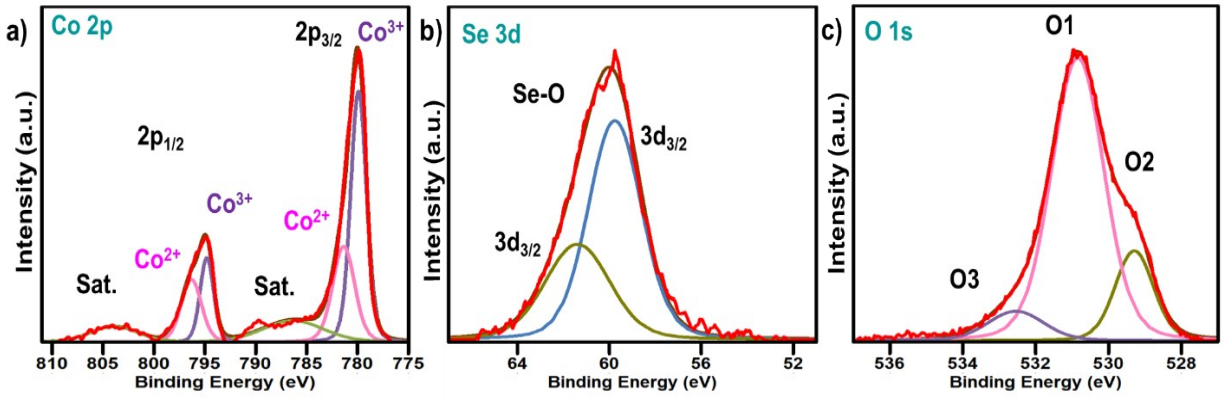

Figure S20. Post GOR catalysis characterization via XPS (a) Co 2p, (b) Se 3d, (c) O 1s.

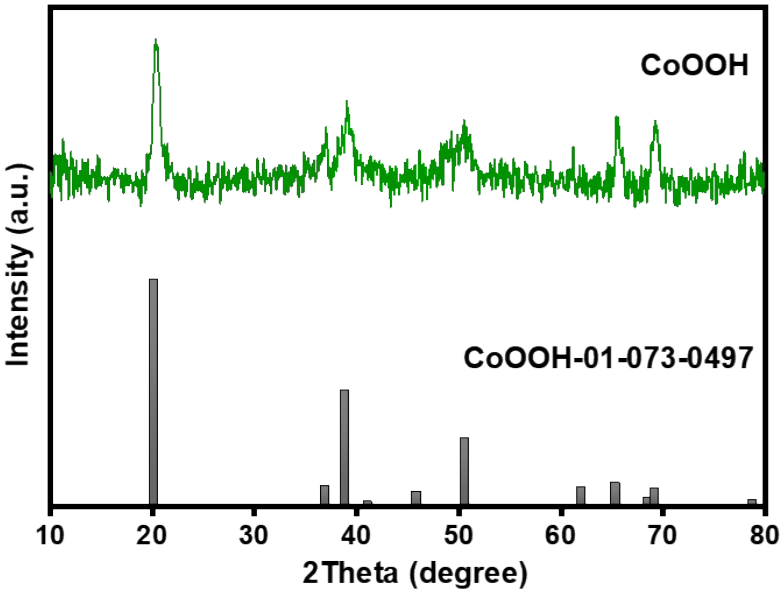

Figure S21. PXRD pattern for the conventional CoOOH synthesized.

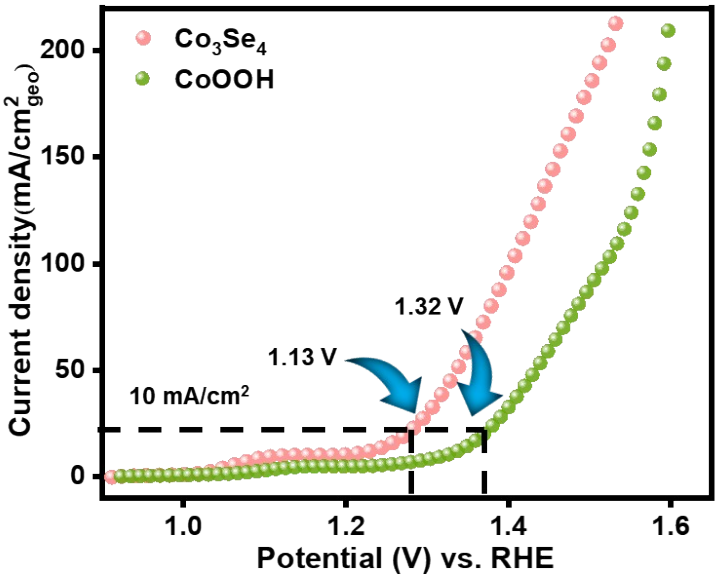

Figure S22. Comparison of the activity of conventional CoOOH with Co_3Se_4 for GOR.

Computational data for GOR

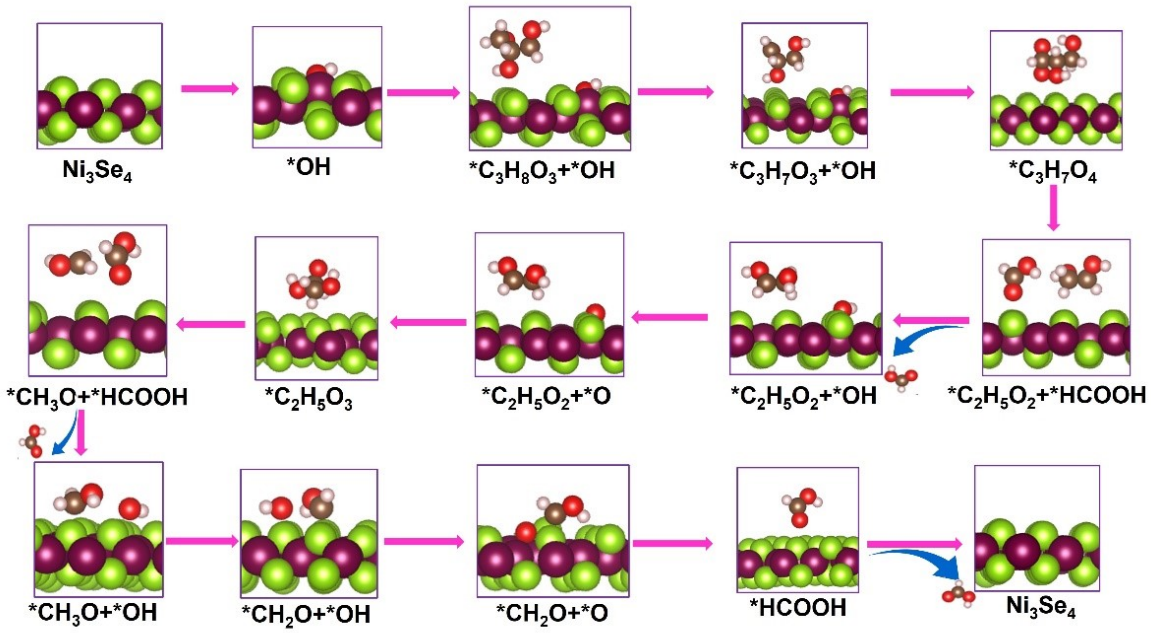

Figure S23: The optimized geometries of all the steps in the glycerol oxidation mechanism on the Ni_3Se_4 surface.

Experimental data for HzOR

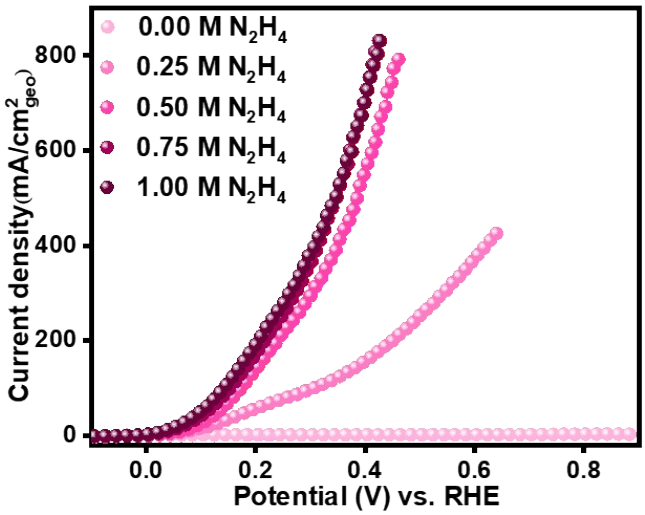

Figure S24. LSV curves of Co_3Se_4 without hydrazine and at different hydrazine concentrations.

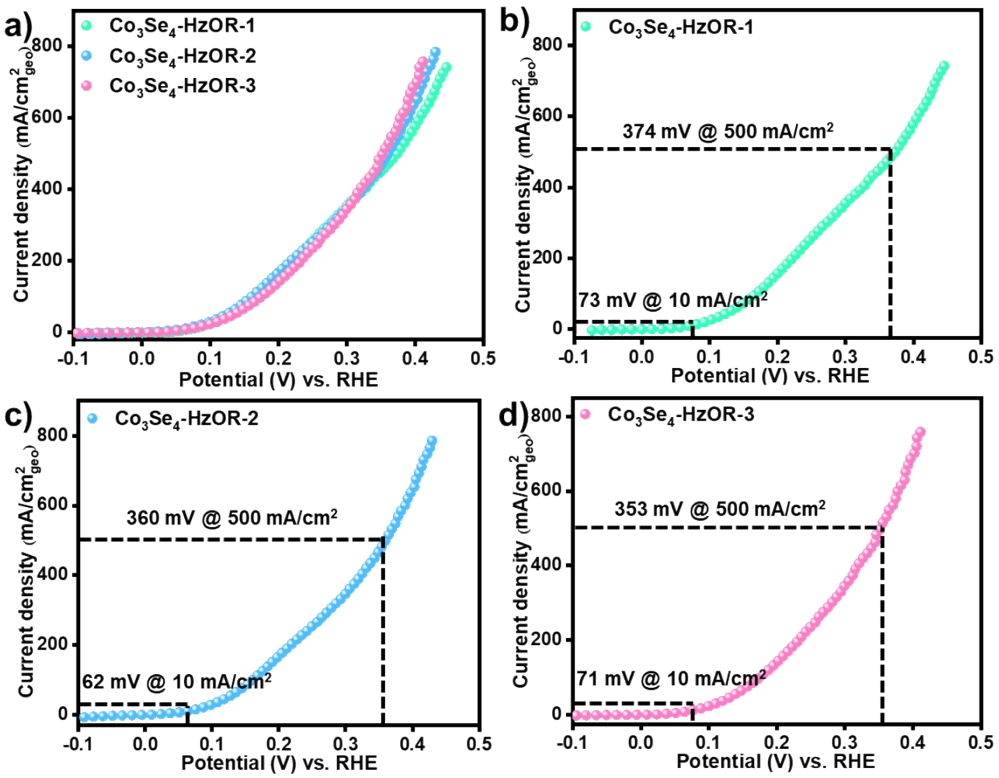

Figure S25. Reproducibility of electrocatalytic performance of Co_3Se_4 toward HzOR in 0.75 M N_2H_4 + 1 M KOH with a standard deviation of 6 mV and 11 mV at 10 and 500 mA/cm^2, respectively.

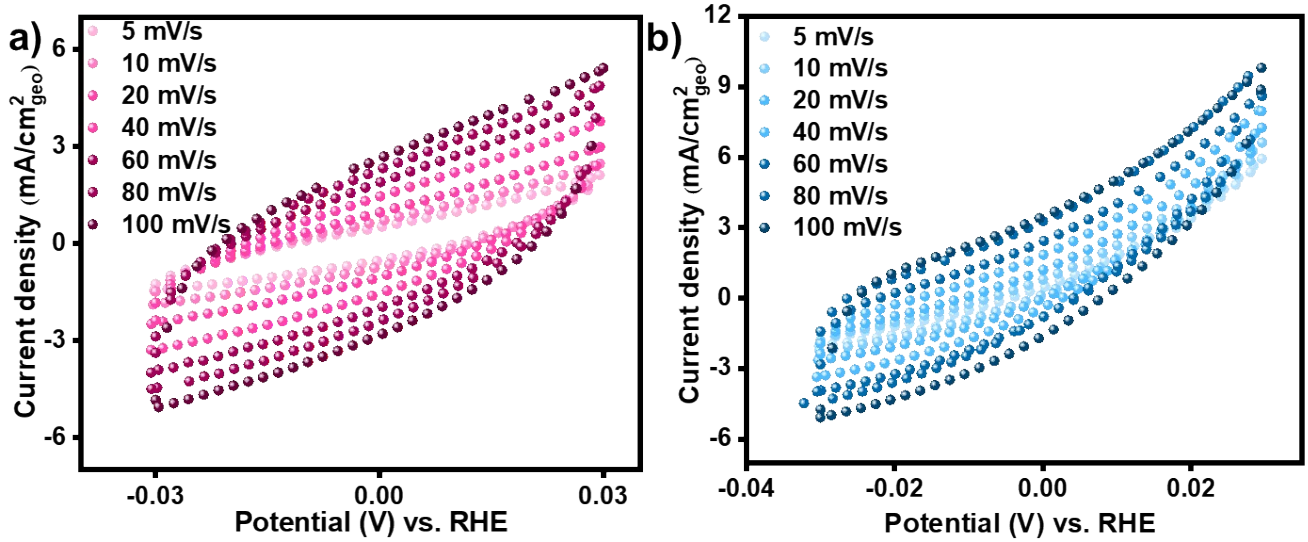

Figure S26. CVs of (a) Co_3Se_4 and (b) Ni_3Se_4 for HzOR at different scan rates and in the non-faradaic potential region.

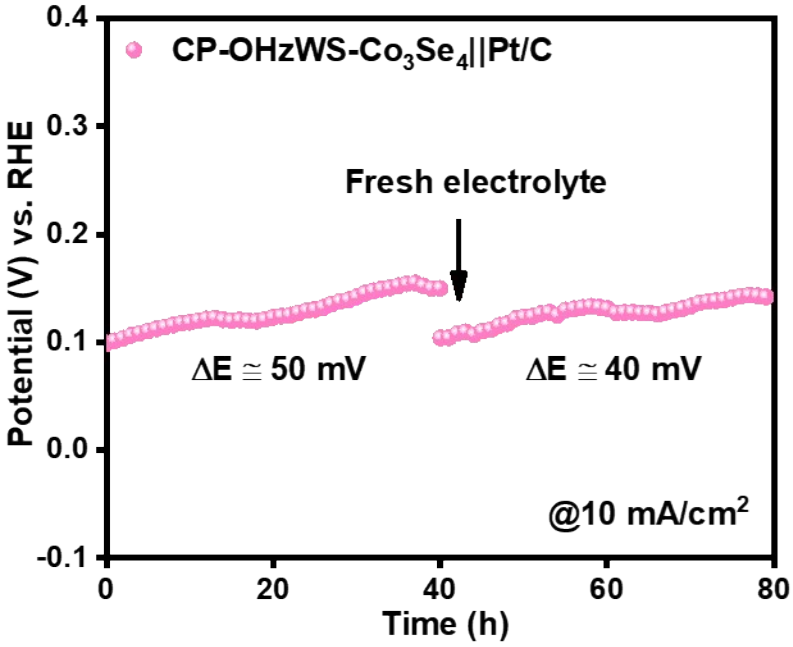

Figure S27. Chronopotentiometry test of Co_3Se_4 || Pt/C for OHzWS for 80 h at 10 mA/cm^2.

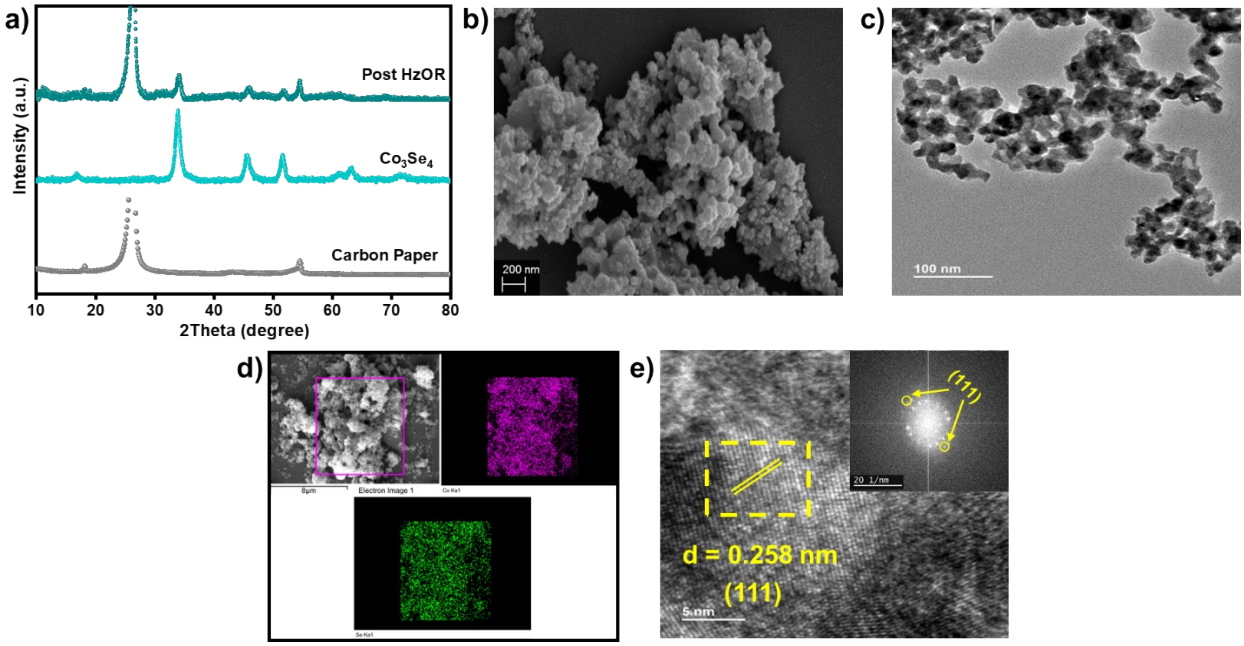

Figure S28. Post HzOR catalysis characterization via (a) PXRD, (b) SEM, (c) TEM, (d) Elemental mapping, (e) HR-TEM (inset: Corresponding FFT).

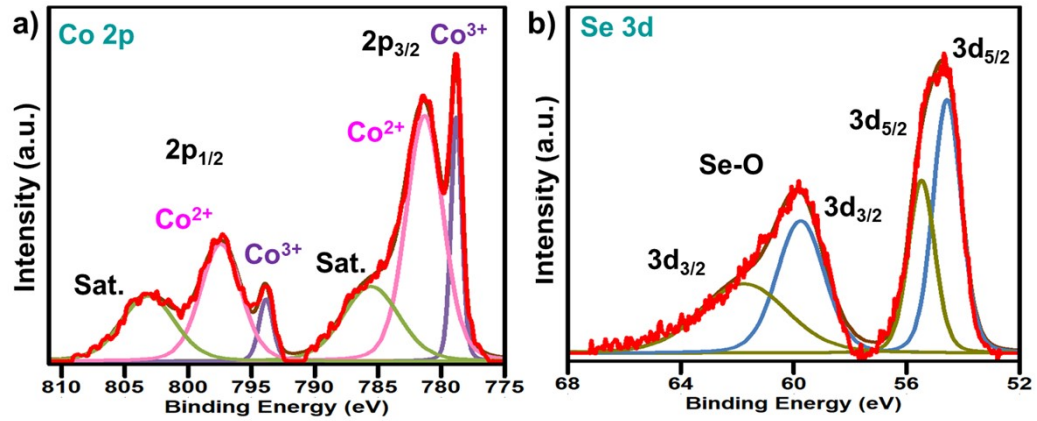

Figure S29. Post GOR catalysis characterization via XPS (a) Co 2p, (b) Se 3d.

Experimental data for the Water oxidation reaction

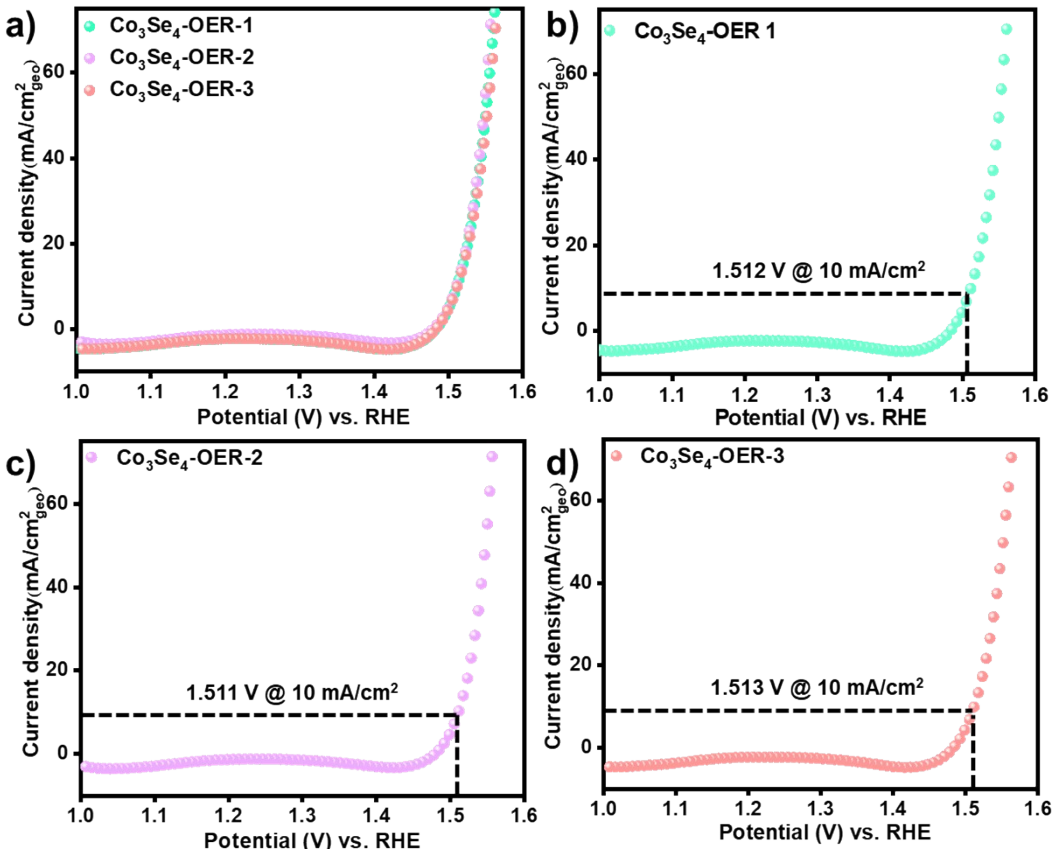

Figure S30. Reproducibility of electrocatalytic performance of Co_3Se_4 toward OER in 1 M KOH with a standard deviation of 1 mV at 10 mA/cm^2.

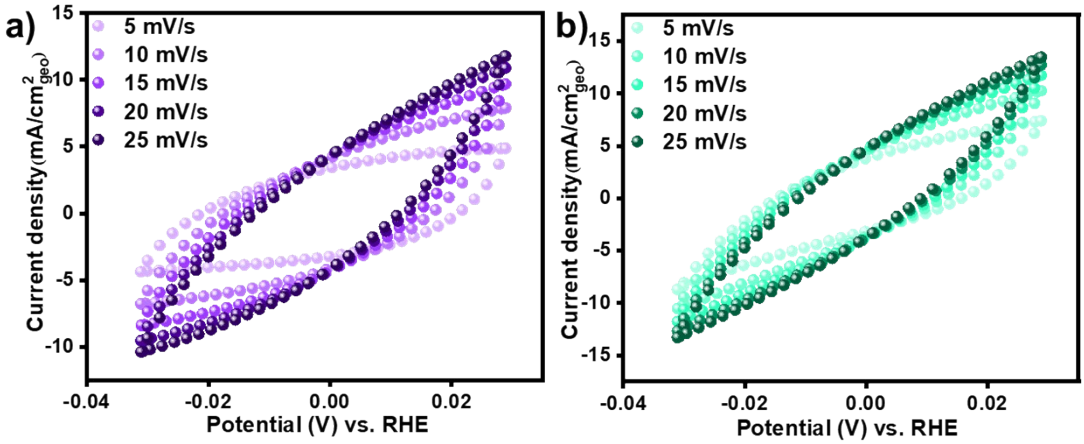

Figure S31. CVs of (a) Co_3Se_4 and (b) Ni_3Se_4 for OER at different scan rates and in the non-faradaic potential region.

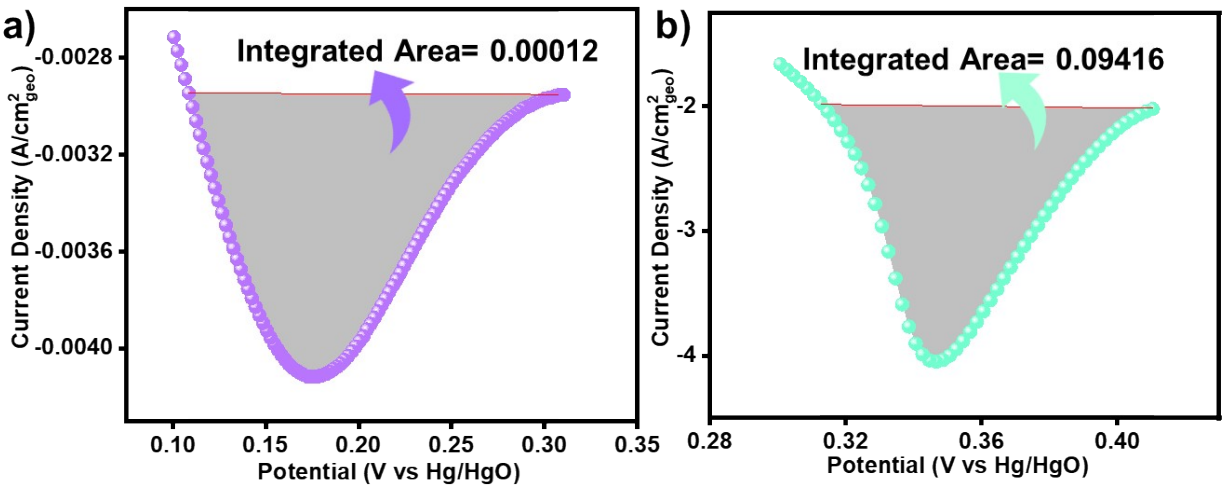

Figure S32. The area under the reduction peak from the CV graph of (a) Co_3Se_4 and (b) Ni_3Se_4.

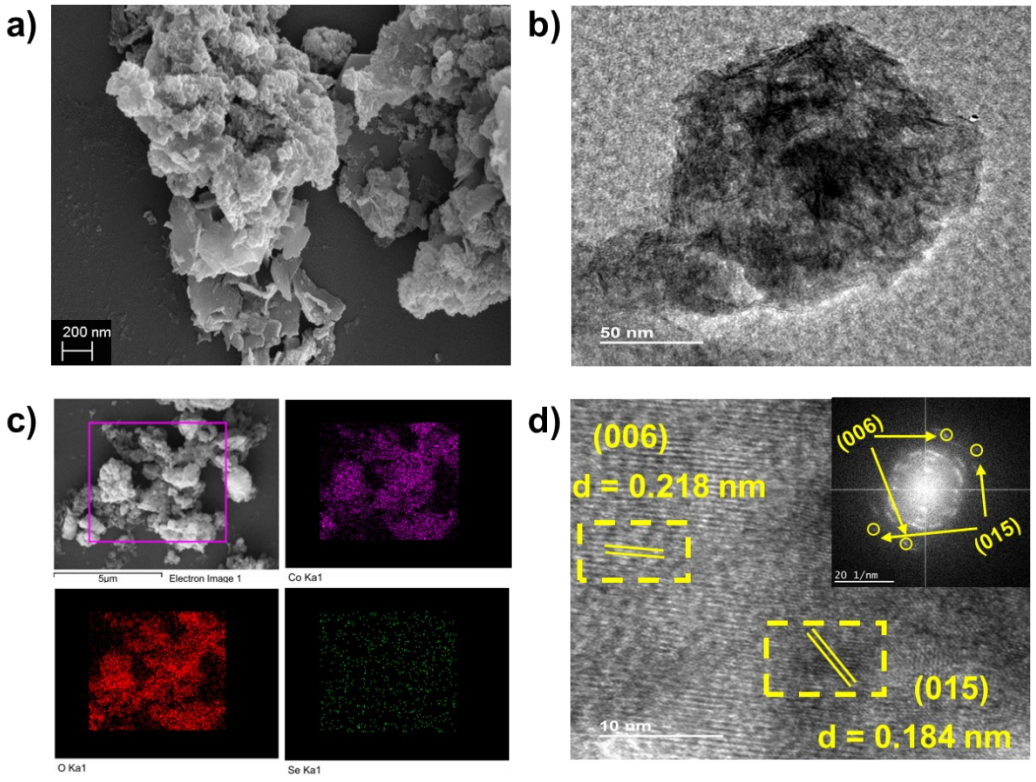

Figure S33. Post OER catalysis characterization via (a) SEM, (b) TEM, (c) Elemental mapping, (d) HR-TEM (inset: Corresponding FFT).

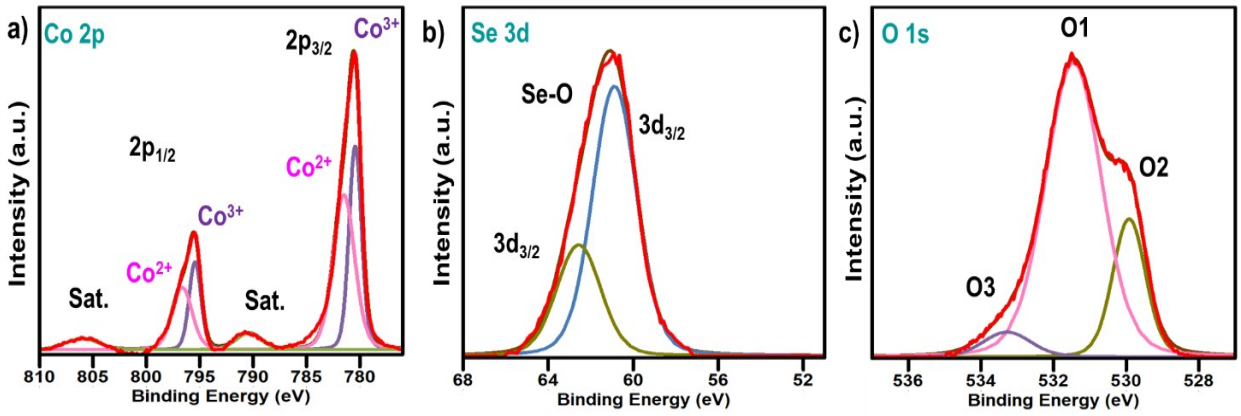

Figure S34. Post OER catalysis characterization via XPS (a) Co 2p, (b) Se 3d (c) O 1s.

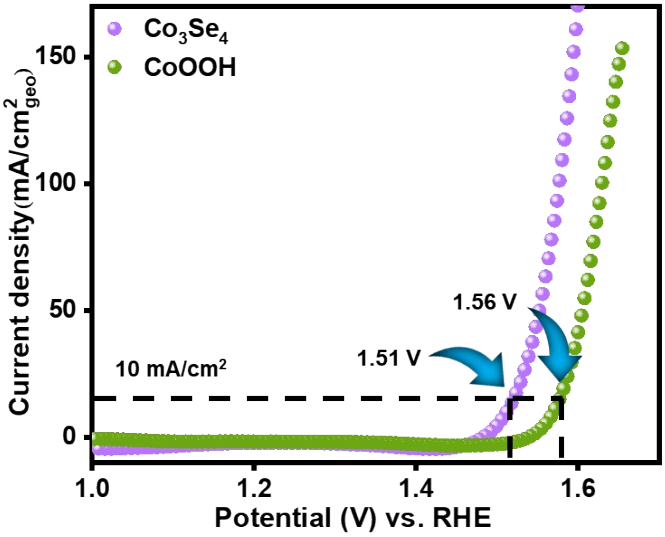

Figure S35. Comparison of activity of conventional CoOOH with Co_3Se_4 for (a) GOR and (b) OER.

Table S1. Comparison table of the GOR activity of Co_3Se_4 with recently reported chalcogenide-based GOR electrocatalysts.

S. N.	Catalysts	Electrolyte	Main products	Voltage value	FE (%)	Ref.
1	Ni-Mo-N/CFC	1.0 M KOH with 0.1 M glycerol	Formate	1.36 V of cell voltage @ 10 mA cm^{-2}	95	Nature Communications,2019, 10, 5335.
2	$CuCo_2O_4$ on carbon fiber paper	0.1 M KOH + 0.1 M glycerol	Formic acid	1.30 V @ 10 mA cm^{-2}	89	ACS Catal., 2020, 10, 12, 6741.
3	CoNi film on Cu rod	0.33 M glycerol in 1 M KOH	-	1.36 V @ 10 mA cm^{-2}	-	International Journal of Hydrogen Energy, 2022, 47, 75, 32145.
4	(CoNiCuMnMo)Se/CF	1 M KOH + 0.1 M glycerol	Formate	1.20 V @ 10 mA cm^{-2}	-	NanoResearch, 2023, 16, 8, 10832.
5	Mo-Co_2P/NF	1 M KOH + 0.1 M glycerol	Formate	1.8 V @ 100 mA cm^{-2}	-	Journal of Colloid and Interface Science, 2024, 665, 152.
6	Ni_3N/WO_3	1 M KOH + 0.1 M glycerol	Formic acid	1.5 V cell voltage @ 100 mA cm^{-2}		ChemSusChem, 2024, e20240062
7	$CoMoO_4$/NF	1 M KOH + 0.1 M glycerol	Formate	1.24 V @ 10 mA cm^{-2}	90	Adv. Energy Mater., 2022, 12, 2103750.
8	Cu–Cu_2O/CC	1 M KOH + 0.5 M glycerol	Formate	1.21 V @ 10 mA cm^{-2}	97	Nanoscale, 2022, 14, 12841.
9	Co_9S_8/NF	1 M KOH + 0.1 M glycerol	Formate	1.30 V onset potential	80	J. Mater. Chem. A, 2024, 12, 30522–30533

10	**Co_3Se_4/CP**	**1.0 M KOH + 0.1 M glycerol**	**Formate**	**1.13 V @ 10 mA cm^{-2}**	**76**	**This work**

Table S2. Comparison table of the HzOR activity of Co_3Se_4 with recently reported chalcogenide-based HzOR electrocatalysts.

S.N.	Catalysts	Substrate	Electrolyte (xM Hydrazine +yM KOH)	Current density (mA/cm^2)	Voltage (V) vs RHE	Ref.
1	Ni_3S_2	Ni foam	0.2 M +1.0 M	100	0.415	J. Mater. Chem. A, 2018, 6, 19201.
2	$Ni_{0.6}Co_{0.4}Se$	Ni Foam	0.1 M +1.0 M	300	0.400	Nanoscale, 2020, 12, 4426
3	Ni_3Se_4	Ni Foam	0.1 M +1.0 M	10	0.320	J. Mater. Chem. A, 2018, 6, 32
4	$NiCoSe_2$	Ni Foam	0.1 M + 0.5M	50	-0.4 (SCE)	ACS Sustain. Chem. Eng., 2018, 6, 7735
5	S-CuNiCo LDH	Ni foam	0.02 M + 0.1 M	50	0.45	J. Mater. Chem. A, 2019, 7, 24437.
6	$Co_{0.5}NiS$	Ni Foam	0.5 M +1.0 M	50	0.270	Adv. Funct. Mater., 2024, 34, 2310288
7	NiCo alloy @ NiCoS	Ni foil	0.02 M+0.1M	10	0.800	Adv. Mater., 2017, 29, 1604080
8	Fe-CoS_2	Glassy Carbon	0.1 M +1.0 M	100	0.129	Nat. Commun., 2018, 9, 1
						Int. J.

9	CoFeNiSOH	Ni Foam	0.4 M +1.0 M	100	0.355	Hydrogen Energy, 2024, 49
10	P-$NiCo_2S_4$	Carbon paper	0.5 M +1.0 M	300	0.700	Inorg. Chem., 2023, 62, 39
11	$NiCo_2S_4$	Carbon paper	0.5 M+1.0 M	10	0.153	ChemCatChem, **2025**, 17, e202401773
12	**Co_3Se_4**	**Carbon paper**	**0.75 M+1.0 M**	**10**	**0.071**	**This work**
				100	**0.174**	
				500	**0.352**	

Table S3. Comparison table of the OER activity of Co_3Se_4 with recently reported chalcogenide-based OER electrocatalysts.

S. N.	**Catalysts**	**Substrate**	**Electrolyte**	**Current density (mA/cm^2)**	**Overpotential (V) vs RHE**	**Ref.**
1	Hierarchical Porous Ni_3S_4	Nickel foam	1 M KOH	10	0.257 (From forward scan) 0.307 (From backward scan)	Adv. Funct. Mater., 2019, 29, 1900315
2	NiS	Nickel foam	0.1 M KOH	50	0.335 (From forward scan)	Chem. Commun., 2016, 52, 1486
3	Au-$CoNiS_x$	Nickel foam	1 M KOH	10	0.305 (From backward scan)	ACS Appl. Nano Mater., 2024, 7, 8, 9062
4	$NiCo_2Se_4$	Carbon paper	1 M KOH	10	0.330 (From forward scan)	Journal of The Electrochemical Society, 2020, 167,

						056503
5	$NiCo_2S_4$	Glassy Carbon	1 M KOH	10	0.330 (From forward scan)	ACS Appl. Mater. Interfaces, 2017, 9, 2500
6	Ni-based MOF modified Ni_3S_2/NiS hollow nanoparticle	Glassy carbon	1 M KOH	10	0.298 (From forward scan)	ACS Appl. Mater. Interfaces, 2019, 11, 23180
7	$NiCo_2Se_4$	Carbon paper	1 M KOH	10	0.320 (From backward scan)	Inorganic Chemistry, 2021, 60, 9542
8	$NiCo_2S_4$ Nanowire	Nickel foam	1 M KOH	10	0.260 (From forward scan)	Adv. Funct. Mater., 2016, 26, 4661
9	$NiCo_2Se_4$/$NiCo_2S_4$	Carbon cloth	1 M KOH	10	0.330 (From forward scan)	Electrochimica Acta, 2021, 368, 137584
10	CoSe	Glassy carbon	1 M KOH	10	0.295 (From backward scan)	Electrochim. Acta., 2016, 194, 59
11	P-$NiCo_2S_4$	Nickel foam	1 M KOH	50	0.300 (From forward scan)	Electrochimica Acta, 2021, 396, 139236
12	$NiCo_2S_4$	Carbon paper	1 M KOH	10	0.290 (From backward scan)	
13	**Co_3Se_4**	**Carbon paper**	**1 M KOH**	**10**	**0.281** (From backward scan)	**This work**
				50	**0.317** (From backward scan)	